Cryo-EM structure and rRNA model of a translating eukaryotic 80S ribosome at 5.5-Å resolution

Jean-Paul Armache[a,1], Alexander Jarasch[a,1], Andreas M. Anger[a,1], Elizabeth Villa[b], Thomas Becker[a], Shashi Bhushan[a], Fabrice Jossinet[c], Michael Habeck[d,e], Gülcin Dindar[a], Sibylle Franckenberg[a], Viter Marquez[a], Thorsten Mielke[f,g], Michael Thomm[h], Otto Berninghausen[a], Birgitta Beatrix[a], Johannes Söding[a], Eric Westhof[c], Daniel N. Wilson[a,2], and Roland Beckmann[a,2]

[a]Gene Center and Center for Integrated Protein Science Munich, Department of Biochemistry, Ludwig-Maximilians-Universität München, Feodor-Lynen-Strasse 25, 81377 Munich, Germany; [b]Department of Molecular Structural Biology, Max Planck Institute of Biochemistry, Am Klopferspitz 18, 82152 Martinsried, Germany; [c]University de Strasbourg, Institut de Biologie Moleculaire et Cellulaire du Centre National de la Recherche Scientifique, 15 Rue René Descartes, 67084 Strasbourg, France; [d]Department of Empirical Inference, Max Planck Institute for Biological Cybernetics, Spemannstrasse 38, 72076 Tübingen, Germany; [e]Department of Protein Evolution, Max Planck Institute for Developmental Biology, Spemannstrasse 35, 72076 Tübingen, Germany; [f]UltraStrukturNetzwerk, Max Planck Institute for Molecular Genetics, Ihnestrasse 73, 14195 Berlin, Germany; [g]Institut für Medizinische Physik und Biophysik, Charité, Ziegelstrasse 5-8, 10117 Berlin, Germany; and [h]Universität Regensburg, Lehrstuhl für Mikrobiologie, Universitätstrasse 31, 93053 Regensburg, Germany

Edited* by Gunter Blobel, The Rockefeller University, New York, NY, and approved September 8, 2010 (received for review July 9, 2010)

Protein biosynthesis, the translation of the genetic code into polypeptides, occurs on ribonucleoprotein particles called ribosomes. Although X-ray structures of bacterial ribosomes are available, high-resolution structures of eukaryotic 80S ribosomes are lacking. Using cryoelectron microscopy and single-particle reconstruction, we have determined the structure of a translating plant (*Triticum aestivum*) 80S ribosome at 5.5-Å resolution. This map, together with a 6.1-Å map of a *Saccharomyces cerevisiae* 80S ribosome, has enabled us to model ∼98% of the rRNA. Accurate assignment of the rRNA expansion segments (ES) and variable regions has revealed unique ES–ES and r-protein–ES interactions, providing insight into the structure and evolution of the eukaryotic ribosome.

modeling | molecular dynamics | flexible fitting

In all living cells, the translation of mRNA into polypeptide occurs on ribosomes. Ribosomes provide a platform upon which aminoacyl-tRNAs interact with the mRNA as well as position the aminoacyl-tRNAs for peptide-bond formation (1). Ribosomes are composed of two subunits, a small subunit that monitors the mRNA–tRNA codon-anticodon duplex to ensure fidelity of decoding (2, 3) and a large subunit that contains the active site where peptide-bond formation occurs (4). Both the small and large subunits are composed of RNA and protein: In eubacteria such as *Escherichia coli*, the small subunit contains one 16S rRNA and 21 ribosomal proteins (r proteins), whereas the large subunit contains 5S and 23S rRNAs and 33 r proteins. Crystal structures of the complete bacterial 70S ribosome were initially reported at 5.5 Å (5), with an interpretation based on atomic models of the individual subunit structures (6–8), and are now available at atomic resolution (9). These structures have provided unparalleled insight into the mechanism of different steps of translation (1) as well as inhibition by antibiotics (10).

Compared to the bacterial ribosome, the eukaryotic counterpart is more complicated, containing expansion segments (ES) and variable regions in the rRNA as well as many additional r proteins and r-protein extensions. Plant and fungal 80S ribosomes contain ∼5,500 nucleotides (nts) of rRNA and ∼80 r proteins, whereas bacterial 70S ribosomes comprise ∼4,500 nts and 54 r proteins. The additional elements present in eukaryotic ribosomes may reflect the increased complexity of translation regulation in eukaryotic cells, as evident for assembly, translation initiation, and development, as well as the phenomenon of localized translation (11–15).

Early models for eukaryotic ribosomes were derived from electron micrographs of negative-stain or freeze-dried ribosomal particles (16) and localization of r proteins was attempted using immuno-EM and cross-linking approaches; see, for example, refs. 17–20. The first cryo-EM reconstruction of a eukaryotic 80S ribosome was reported for wheat germ (*Triticum aestivum*) at 38 Å (21). Initial core models for the yeast 80S ribosome were built at 15-Å resolution (22) by docking the rRNA structures of the bacterial small 30S subunit (6) and archaeal large 50S subunit (8), as well as docking of corresponding homology models of the r proteins. Recently, reconstructions at about 9-Å resolution of fungal and dog 80S ribosomes were used to extend the molecular models to include rRNA expansion segments (23, 24). However, due to the modest resolution, the completeness and accuracy of these models are also limited.

Here we have determined a cryo-EM structure of a wheat germ (*T. aestivum*) translating 80S ribosome at 5.5-Å resolution, enabling us to systematically model ∼98% of the rRNA. This effort encompasses the de novo modeling of 1,885 nucleotides comprising structurally variable regions and rRNA expansion segments. The model reveals direct interaction between ES3 and ES6 as predicted previously by Alkemar and Nygård (25), as well as r-protein–ES interactions, such as L6e and L28e with $ES7^L$ and L34e and L38e with $ES27^L$. The accurate modeling of the rRNA has enabled the localization of 74 (92.5%) of the 80 r proteins of the 80S ribosome (see ref. 26).

Results and Discussion

Cryo-EM Reconstructions of *T. aestivum* and Yeast 80S Ribosomes. Cryo-EM and single-particle analysis were used to reconstruct the *T. aestivum* translating 80S ribosome (Fig. 1*A*) at 5.5-Å resolution (Fig. S1). Similarly, we have previously reported a cryo-EM structure of a translating *Saccharomyces cerevisiae* 80S ribosome

Author contributions: R.B. designed research; J.-P.A., A.J., A.M.A., E.V., T.B., S.B., F.J., M.H., G.D., S.F., V.M., T.M., O.B., B.B., J.S., E.W., and D.N.W. performed research; ; E.V., F.J., M.H., M.T., J.S., and E.W. contributed new reagents/analytic tools; J.-P.A., A.J., A.M.A., E.V., T.B., F.J., E.W., D.N.W., and R.B. analyzed data; and J.-P.A., A.J., A.M.A., D.N.W., and R.B. wrote the paper.

The authors declare no conflict of interest.

*This Direct Submission article had a prearranged editor.

Freely available online through the PNAS open access option.

Data deposition: Coordinates of the atomic models of yeast and *Triticum aestivum* 80S complex have been deposited in the Protein Data Bank (PDB), www.pdb.org [PBD ID codes 3IZE, 3IZF, 3IZD (yeast rRNA), 3IZB, 3IZC (yeast r-proteins), and 3IZ7, 3IZ9 (*T. aestivum* rRNA), 3IZ6, 3IZ5 (*T. aestivum* r proteins)]. The cryoelectron microscopic map of the *T. aestivum* 80S-RNCs has been deposited in the 3D-Electron Microscopy Data Bank (EMDB, http://www.ebi.ac.uk/pdbe/emdb/) (EBMD ID code EMD-1780).

[1]J.-P.A., A.J., and A.M.A. contributed equally to this work.

[2]To whom correspondence may be addressed. E-mail: beckmann@lmb.uni-muenchen.de or wilson@lmb.uni-muenchen.de.

This article contains supporting information online at www.pnas.org/lookup/suppl/doi:10.1073/pnas.1009999107/-/DCSupplemental.

at 6.1-Å resolution (Fig. 1*B*) (27). For both reconstructions, ribosome-nascent chain complexes in the posttranslocational state were utilized (27, 28), after in silico sorting (see *Experimental Procedures*) to increase conformational homogeneity. The final reconstruction of the *T. aestivum* 80S ribosome was derived from 1,362,920 particles sorted for the presence of peptidyl-tRNA in the P site (Fig. 1*A*). The resulting cryo-EM map displays characteristics similar to X-ray crystallographic maps of ribosomes at similar resolution, namely, the *Haloarcula marismortui* 50S subunit at 5 Å (29) and the *Thermus thermophilus* 30S (30) and 70S structures (5) at 5.5 Å (Fig. 1 *C*–*F*). At this resolution, well-resolved density for double-helical RNA is observed, with defined minor and major grooves as well as distinctive bumps indicative of phosphate groups located along the backbone ridges (Fig. 1 *C* and *D*). In many regions, single-stranded rRNA sections are traceable and assignment of bulged nucleotides is possible, as reported previously for the 5.8-Å cryo-EM map of TnaC-stalled bacterial 70S ribosome (31). For r proteins, α-helices are observed as rod-like densities (Fig. 1*E*) and β-sheets are represented by smooth surfaces (Fig. 1*F*). The α-helix pitch and strand separation for β-sheets are indiscernible, as expected at this resolution.

Near-Complete Models for the *T. aestivum* and Yeast 80S Ribosomes. The majority of the conserved core of the *T. aestivum* and yeast 80S ribosomes was modeled based on homology of the eukaryotic rRNA with the available bacterial and archaeal ribosome structures using Assemble (32). On this basis, it was possible to generate a template-based model for the *T. aestivum* 80S with a total of 3,466 (1,051/40S and 2,415/60S) nts of the 5485 rRNA, incorporating isosteric base substitutions (33) (Fig. 2). Nucleotides that were not available in the sequences for *T. aestivum* (120 nts, 2.2%) were substituted with those from the closely related *Oryza sativa*. One-hundred sixteen (67 and 49) nts, mostly single-stranded linker regions, could not be modeled (orange in Fig. 2 *A* and *B*; enlargement in Figs. S2–S7) due to unreliable secondary structure predictions and/or ambiguity in the electron density. The remaining 1,903 nts comprising structurally variable regions and rRNA expansion segments were modeled de novo (green in Fig. 2 *A*–*D*) using Assemble (32), RNAfold (34), and RNAshapes (35). Similarly, models for 44 of the 80 r proteins of the *T. aestivum* 80S ribosome (gray in Fig. 2 *E* and *F*) were built using the templates present in the bacterial and archaeal ribosome structures (29, 30), as well as 44 of 79 r proteins of the yeast 80S ribosome (see ref. 26). Models were fitted into the density using Molecular Dynamics Flexible Fitting (MDFF) (36). The *T. aestivum* and yeast 80S models contain all five expansion segments (ES3^S, ES6^S, ES7^S, ES9^S, and ES12^S following the ES nomenclature of ref. 37) and five variable regions (h6, h16, h17, h33, and h41) of the small subunit, as well as the 16 expansion segments (ES3^L, ES4^L, ES5^L, ES7^L, ES9^L, ES10^L, ES12^L, ES15^L, ES19^L, ES20^L, ES24^L, ES26^L, ES27^L, ES31^L, ES39^L, and ES41^L) and two variable regions (H16–18 and H38) of the large subunit (Fig. 3). On the small subunit, the majority of the additional rRNA is clustered at the spur or foot region, except for ES9^S which is positioned at the head (Fig. 3 *C* and *E*). On the large subunit, most ES are located on the back and sides of the particle, leaving the subunit interface and exit tunnel regions essentially unaffected (Fig. 3 *D* and *F*).

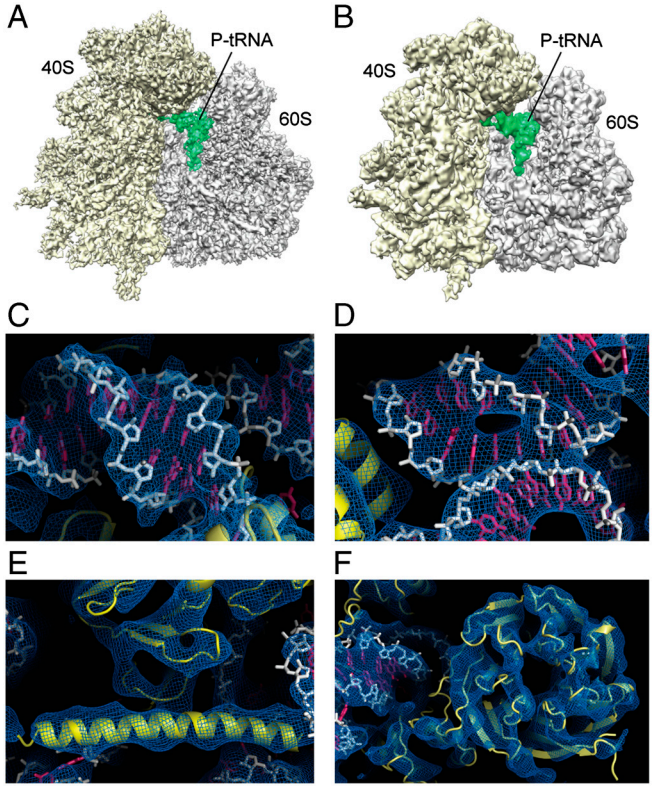

Fig. 1. Cryo-EM reconstruction of eukaryotic 80S ribosomes. (*A*) *T. aestivum* and (*B*) *S. cerevisiae* 80S ribosomes, with small (40S) and large (60S) subunits colored yellow and gray, respectively and the P-tRNA, green. (*C*–*F*) Selected views of the *T. aestivum* 80S density map (blue mesh) and corresponding molecular model, with r protein in yellow and rRNA in white (backbone) and red (bases).

Comparison of Expansion Segments Between Yeast and Wheat Germ. Interestingly, the density maps of the *T. aestivum* and yeast 80S reconstructions support a direct interaction of the loop of ES6^{S}d with the internal loop between ES3^{S}b and ES3^{S}c (Fig. 4*A*), as predicted previously by Alkemar and Nygård (25). Although this interaction was not modeled in the fungal or canine 80S ribosomes (23, 24), covariation analysis suggests that the ES3^S–ES6^S base-pairing interaction is also conserved in mammalian 80S ribosomes (25).

The largest ES in the *T. aestivum* and yeast ribosomes is ES7^L, which is located at the back of the 60S subunit (Fig. 4*B*). Overall, ES7^L is similar between *T. aestivum* and yeast, however, at least two clear differences are evident: Firstly, density for ES7^{L}a in yeast is only seen at low thresholds (Fig. S8), suggesting it is more flexible than in *T. aestivum* (Fig. 4*B*). The reason for this flexibility appears to be that ES7^{L}a in *T. aestivum* is stabilized through an interaction with r-protein L28e (Fig. 4*B*), which is not present in the *S. cerevisiae* genome (38). Secondly, *T. aestivum* contains a three-way junction formed by ES7^{L}c–e, whereas this architecture is not present in yeast due to the absence of ES7^{L}d,e (Fig. 4*B* and Figs. S2–S7). Surprisingly, the N terminus of *T. aestivum* r-protein L6e, which is shorter in yeast, appears to insert through the three-way junction of ES7^L (Fig. 4*B*), an RNA-protein interaction that has to our knowledge not been reported previously.

ES27^L is unique for its highly dynamic behavior, being found in two distinct positions in yeast 80S ribosomes (39); one oriented toward the L1 stalk, termed ES27$^L_{in}$ and one away from the L1 stalk but toward the tunnel exit, termed ES27$^L_{out}$ (Fig. 4*C*). Modeling of both conformations reveals that interchange between the ES27$^L_{in}$ (gold) and ES27$^L_{out}$ (blue) positions involves a rotation of ~110° of ES27^{L}a–c relative to H63 (Fig. 4*C*). Weak density for ES27^L in the reconstruction of the *T. aestivum* ribosome suggests that ES27^L exhibits a continuum of different conformational states. Nevertheless, at low thresholds, one preferential state is observed, intermediate in position (ES27$^L_{int}$) to the yeast ES27$^L_{in}$ and ES27$^L_{out}$ positions (Fig. 4*C* and Fig. S8). All three positions appear to be stabilized through interaction with newly identified eukaryotic-specific r proteins: The yeast ES27$^L_{out}$ and the *T. aestivum* ES27$^L_{int}$ conformations directly contact r-protein L38e (Fig. 4*C*), whereas r-protein L34e stabilizes the yeast ES27$^L_{in}$ position. In *Tetrahymena*, deletion of

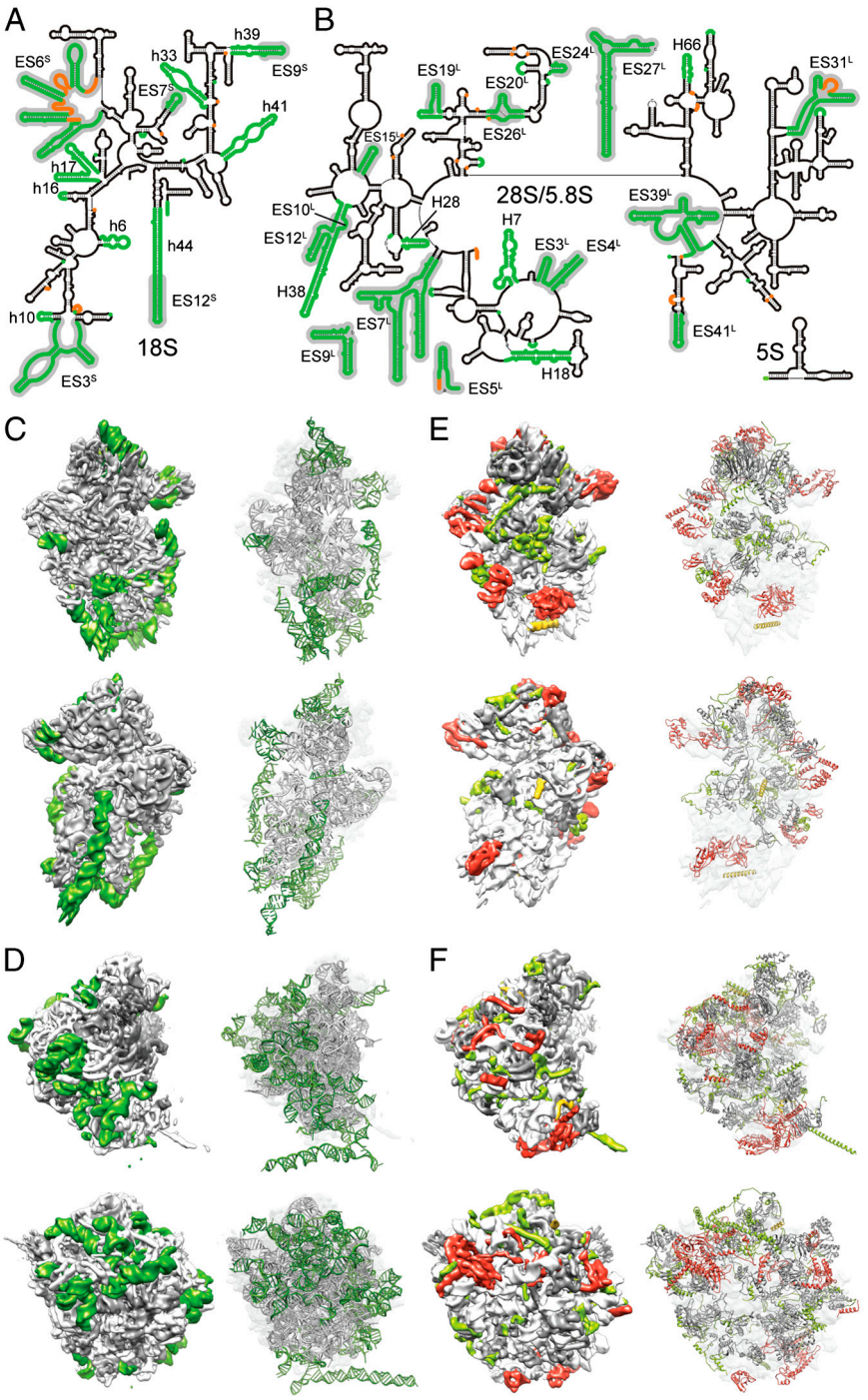

Fig. 2. An atomic model for the *T. aestivum* 80S ribosome. (*A* and *B*) Secondary structures for the (*A*) small (18S) and (*B*) large subunit (5S, 5.8S, and 28S) ribosomal RNAs, with the newly modeled regions colored green. Expansion segments and variable regions are indicated in gray and unmodeled regions are orange. (*C* and *D*) Newly modeled regions of rRNA (green) are highlighted on the (*C*) small and (*D*) large subunit density map (*Left*) and as molecular models (*Right*). (*E* and *F*) Newly modeled proteins are highlighted on the (*E*) small and (*D*) large subunit density map (*Left*) and as molecular models (*Right*). Newly identified proteins are colored red, whereas de novo modeled extensions are colored light green, and modeled but unassigned proteins are yellow.

ES27^{L} is lethal (40), suggesting a functionally important role for this RNA insertion. Despite the high variability in length of ES27^{L}, ranging from ∼150 nucleotides in *T. aestivum* and yeast to ∼700 nucleotides in mammals (41), the ES27^{L} deletion can be complemented with a corresponding ES27^{L} from other species (40). ES27^{L} has been suggested to play a role in coordinating the access of nonribosomal factors at the tunnel exit (39).

Evaluation of RNA Models for the Eukaryotic Ribosome. A reconstruction at 8.7 Å of a canine ribosome was used for a model including models of ∼50% of the ES by fitting of A-form helices into the ES density (23). Recently, a more comprehensive model of the yeast *S. cerevisiae* ribosome was built on the basis of an 8.9-Å cryo-EM reconstruction of a 80S ribosome from a related thermophilic fungus, *Thermomyces lanuginosus* (24), which, however, shares only ∼85% sequence identity with *S. cerevisiae* rRNA. With the exception of ES10^{L}, ES27^{L}, and the tip of ES15^{L}, molecular models were built for all the remaining expansion segments and variable regions (24). Yet, a number of significant differences between the yeast model presented by Taylor et al. (24) and the

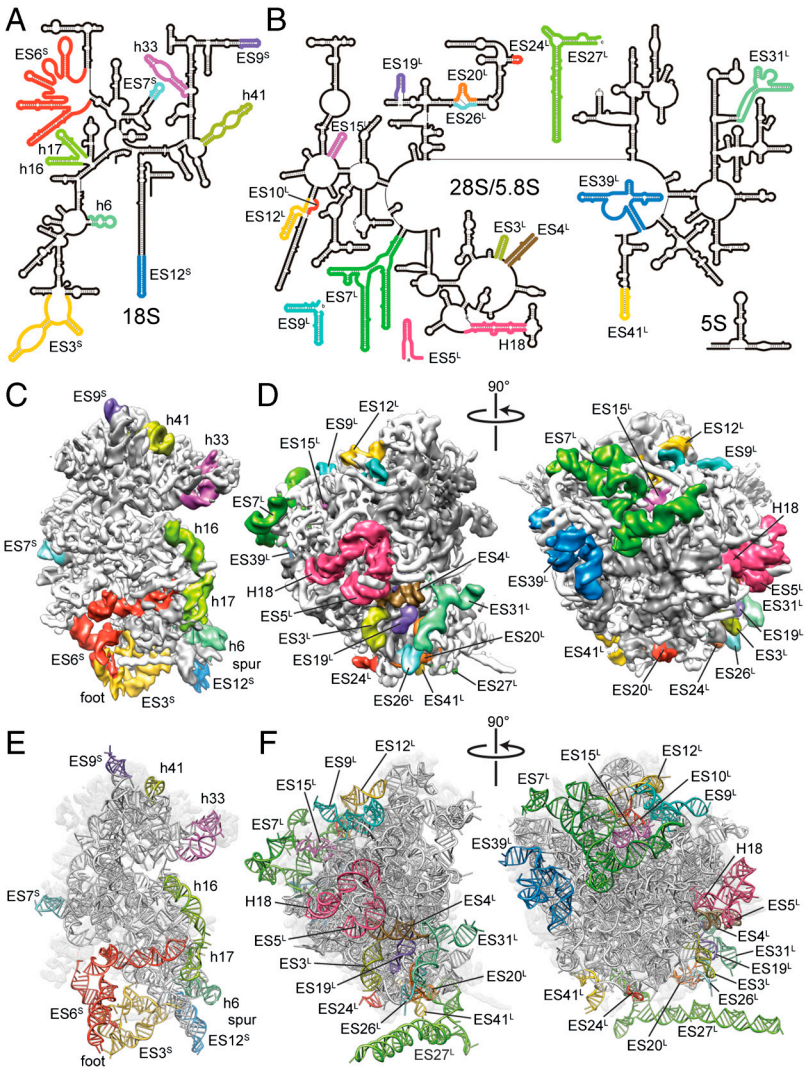

Fig. 3. Ribosomal RNA expansion segments and variable regions. (*A* and *B*) Secondary structures for the *T. aestivum* (*A*) small (18S) and (*B*) large subunit (5S, 5.8S, and 28S) ribosomal RNAs, with the ES and variable regions (VR) colored distinctly. (*C* and *D*) Cryo-EM maps of the (*C*) small and (*D*) large subunits with assigned ES and VR colored as in *A* and *B*. (*E* and *F*) Molecular models of the ES and VR of rRNA colored as in *C* and *D*.

yeast model presented here are evident (Fig. S9). Taken together, using the correct sequences for modeling into corresponding maps of improved resolution allowed for a significant improvement in completeness and accuracy of both the RNA and protein models.

Evolution of RNA Expansion Segments. A comparison of genomic sequences from diverse organisms, ranging from bacteria to mammals, indicates additional mass with increasing organism complexity (Fig. 5). However, the composition of mammalian ribosomes, e.g., from human, is surprisingly similar to those of other eukaryotes, such as yeast and plants described here. Human ribosomes have the same 80 r proteins that are found in *T. aestivum* ribosomes and, in terms of rRNA, differ significantly only in the length of four ES on the large subunit ($ES7^L$, $ES15^L$, $ES27^L$, and $ES39^L$). These are longer in human (~850, ~180, ~700, and ~220 nts) than in *T. aestivum*/yeast (~200, ~20, ~150, and ~120 nts, respectively), and cryo-EM reconstructions of mammalian ribosomes (23, 42–44) show that the longer ES in mammalian ribosomes are generally highly mobile elements for which little to no density is visible (Fig. 5). Evolution has thus favored the development of two apparently distinct layers of mass gain for the ribosome: A first layer of tightly intertwined additional proteins and rRNA expansions rigidly positioned on the subunit surfaces (with the only exception of the mobile $ES27^L$), which was followed by a second layer comprising a few drastically extended highly mobile rRNA elements with hitherto unknown function.

Experimental Procedures

Sample Preparation and Cryo-EM. The cryo-EM map used for modeling of the yeast 80S ribosome was previously deposited in the Electron Microscopy Data Bank (EMDB ID 1669; ref. 27). *T. aestivum* ribosome nascent chain complexes (RNCs) were generated using a homemade wheat germ in vitro translation system (based on ref. 45) and were purified according to ref. 46. As described previously (47), *T. aestivum* RNC samples were applied to carbon-coated holey grids, and micrographs were recorded under low-dose conditions on a Polara field emission gun electron microscope at 300 kV (FEI) in a defocus range of 1.0–4.5 μm. Micrographs were scanned on a Heidelberg Primescan D8200 drum scanner, resulting in a pixel size of 1.24 Å on the object scale. The data were analyzed by determination of the contrast transfer function using CTFFIND (48). The data were further processed with the SPIDER software package (49). After automated particle picking followed by visual inspection, 2,108,230 particles of the *T. aestivum* RNC dataset were sorted in a supervised manner (50) into programmed (with

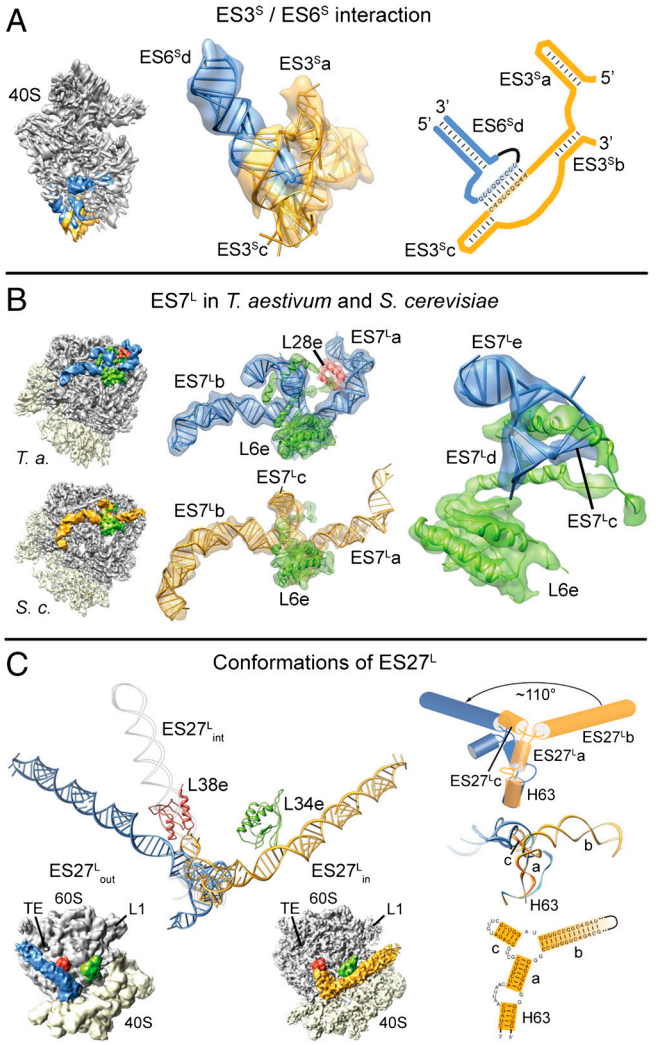

Fig. 4. Molecular models for expansion segments ES3^S/ES6^S, ES7^L, and ES27^L. (*A*) Isolated density for ES6^{S}d (blue) and ES3^{S}a,c (gold) on the 40S subunit (*Left*) and transparent with a molecular model (*Center*). rRNA secondary structure prediction highlighting interaction between the loop of ES6^{S}d and the bulge in ES3^{S}c (*Right*), as proposed by ref. 59. (*B*) Isolated density for ES7^L from *T. aestivum* (*T. a.*, blue) and *S. cerevisiae* (*S. c.*, gold) on the 80S ribosome (*Left*) and transparent with a molecular model (*Center*). Ribosomal proteins L28e (red) stabilizes ES7^{L}a in the *T. aestivum* 80S ribosome, whereas the extension of r-protein L6e appears to pass through the three-way junction formed by helices ES7^{L}c–e (*Right*). Molecular models for the ES27$^L_{in}$ (gold) and ES27$^L_{out}$ (blue) positions (*Left*), as observed in *S. cerevisiae* 80S ribosomes (*Thumbnail Insets*) (39) and an intermediate position (ES27$^L_{int}$, gray) observed in the *T. aestivum* 80S ribosome. In yeast, r-protein L34e (green) and L38e (red) interact with the ES27$^L_{in}$ and ES27$^L_{out}$ positions, respectively. The tunnel exit (TE) and L1 stalk (L1) are indicated for reference. (*C*) Schematic (*Top Right*) and molecular model (*Middle Right*) indicating that the interchange between the ES27$^L_{in}$ (gold) and ES27$^L_{out}$ (blue) positions involves a rotation of ~110° of ES27^{L}a–c relative to H63. Secondary structure for the junctions of *S. cerevisiae* ES27^{L}a–c and H63.

P-tRNA) and unprogrammed/empty (without P-tRNA) ribosome subdatasets, using reconstructions of programmed and unprogrammed ribosomes as initial references. Removal of unprogrammed ribosome particles resulted in 1,362,920 particles that were used for reconstruction of the wheat germ 80S ribosome. The final contrast transfer function corrected reconstruction has a resolution of 5.5 Å, based on the Fourier Shell Correlation with a cutoff value of 0.5 (Fig. S1). Densities for the 40S subunit, the 60S subunit, and the P-site tRNA were isolated using binary masks.

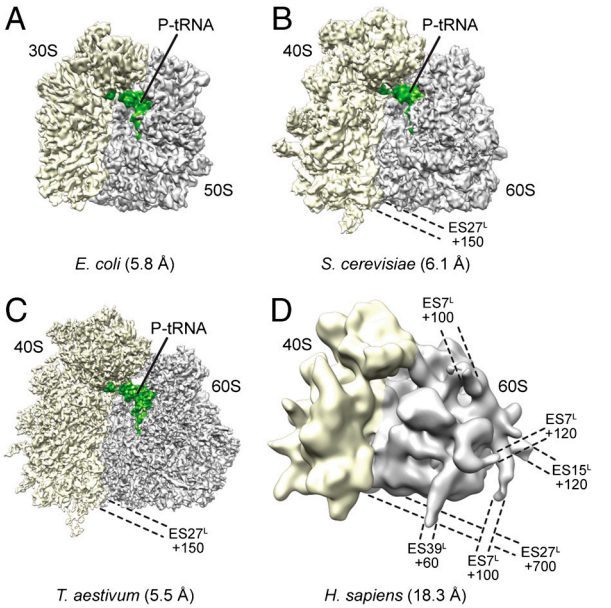

Fig. 5. Cryo-EM reconstructions of ribosomes from (*A*) the eubacterium *Escherichia coli* (31), (*B*) the yeast *S. cerevisiae* (27), (*C*) wheat germ *T. aestivum* (this work), and (*D*) *Homo sapiens* (44). The small and large subunits are shown in yellow and gray, respectively and the P-tRNA (green) is indicated for reference. The dashed lines and numbers indicate the number of nucleotides of the rRNA expansion segments that are not visualized.

Ribosomal RNA Sequences. The rRNA sequences of the *S. cerevisiae* 5S, 5.8S, 18S, and 25S were taken from GenBank Accession number (Acc.) U53879. The rRNA sequence for the *T. aestivum* 5S (Acc. X06094), 5.8S (Acc. FM998894), 18S (Acc. AY049040), and 28S (Acc. AY049041) rRNAs were available, with the exception of five and four nucleotides at the 5′ end of the 18S and 28S, respectively, 46 nts from the 3′ end of the 28S, and 65 nts (487–551) in the 28S corresponding to ES7, which were filled with the corresponding sequences of *O. sativa* (Acc. M11585). Sequence alignments between the available *T. aestivum* and *O. sativa* rRNAs show a 98% sequence identity, indicating the suitability of using the *O. sativa* sequence for filling the missing 120 (2.2%) nucleotides in the *T. aestivum* model.

Modeling of the Ribosomal RNA Core. The structure-based sequence alignment of both the 18S of the small subunit and the 5S, 5.8S, and 28S rRNA of the large subunit was done using the X-ray structure of the large ribosomal of *H. marismortui* [Protein Data Bank (PDB) 1FFK] (8) and the small ribosomal subunit of *T. thermophilus* (PDB 1J5E) (6). For regions like H5–H7, the stalk base (H42–H43), and the L1 stalk (H76–H78), the X-ray structure of *E. coli* (PDB 3FIK) (51, 52) was used as template. The alignment was constructed semiautomatically using S2S (53). The multiple sequence alignment for the 5S, 5.8S, and 28S was constructed between *H. marismortui*, *T. aestivum*/*O. sativa*, and *S. cerevisiae* and for the 18S between *T. thermophilus*, *T. aestivum*/*O. sativa*, and *S. cerevisiae*, respectively. The resulting core models for *S. cerevisiae* and *T. aestivum* were deduced from the alignments using Assemble (32) and core models consist only of isosteric base substitutions (33, 54).

Modeling of the Ribosomal RNA Expansion Segments. Primary sequences were used as an input for RNA secondary structure prediction tools RNAfold (34) and RNAshapes (35). The core model was used as an anchor point for modeling the ES. According to the secondary structure predictions and the electron density, the ES were constructed semiautomatically using Assemble (32). The applied structural motifs for loops and inner helical

non-Watson-Crick base-pairing motifs were extracted from known structures of the PDB and Structural Classification of RNA database (55).

Refinement and Fitting of the rRNA and r-Proteins into the EM Densities. The de novo modeled RNA parts were initially refined using the internal refinement tool of Assemble. A preliminary rigid body fitting of the models was done without proteins using Chimera (56) with low-pass filtered electron densities. Subsequently, all RNA segments were merged using visual molecular dynamics (VMD) (57), and MDFF (36) was applied to fit the rRNA to the density map while preserving canonical and noncanonical base-pair interactions identified by RNAview. Subsequently, proteins were introduced using VMD, and an extended version of interactive molecular dynamics (58), namely, interactive MDFF, was used to refine the proteins into the density while fixing protein–RNA and protein–protein clashes, followed by an MDFF refinement of the entire 80S model.

Visualization and Figure Preparation. Cryo-EM maps and models were visualized and all figures were generated using VMD (57), Chimera (56), and/or PyMol (http://www.pymol.org).

ACKNOWLEDGMENTS. This research was supported by grants from the Deutsche Forschungsgemeinschaft SFB594 and SFB646 (to R.B.), SFB740 (to T.M.), and WI3285/1-1 (to D.N.W.), by the European Union and Senatsverwaltung für Wissenschaft, Forschung und Kultur Berlin (UltraStructureNetwork, Anwenderzentrum), and a Marie Curie International Incoming Fellowship within the Seventh European Community Framework Programme (E.V.). Computer time for MDFF was provided by the Leibniz-Rechenzentrum.

1. Schmeing TM, Ramakrishnan V (2009) What recent ribosome structures have revealed about the mechanism of translation. *Nature* 461:1234–1242.
2. Ogle JM, Ramakrishnan V (2005) Structural insights into translational fidelity. *Annu Rev Biochem* 74:129–177.
3. Zaher HS, Green R (2009) Fidelity at the molecular level: Lessons from protein synthesis. *Cell* 136:746–762.
4. Simonovic M, Steitz TA (2009) A structural view on the mechanism of the ribosome-catalyzed peptide bond formation. *Biochim Biophys Acta* 1789:612–623.
5. Yusupov MM, et al. (2001) Crystal structure of the ribosome at 5.5 A resolution. *Science* 292:883–896.
6. Wimberly BT, et al. (2000) Structure of the 30S ribosomal subunit. *Nature* 407:327–339.
7. Schluenzen F, et al. (2000) Structure of functionally activated small ribosomal subunit at 3.3 A resolution. *Cell* 102:615–623.
8. Ban N, et al. (2000) The complete atomic structure of the large ribosomal subunit at 2.4 Å resolution. *Science* 289:905–920.
9. Selmer M, et al. (2006) Structure of the 70S ribosome complexed with mRNA and tRNA. *Science* 313:1935–1942.
10. Wilson DN (2009) The A-Z of bacterial translation inhibitors. *Crit Rev Biochem Mol Biol* 44:393–433.
11. Sonenberg N, Hinnebusch AG (2009) Regulation of translation initiation in eukaryotes: Mechanisms and biological targets. *Cell* 136:731–745.
12. Warner JR, McIntosh KB (2009) How common are extraribosomal functions of ribosomal proteins? *Mol Cell* 34:3–11.
13. Freed EF, Bleichert F, Dutca LM, Baserga SJ (2010) When ribosomes go bad: Diseases of ribosome biogenesis. *Mol Biosyst* 6:481–493.
14. Jackson RJ, Hellen CU, Pestova TV (2010) The mechanism of eukaryotic translation initiation and principles of its regulation. *Nat Rev Mol Cell Biol* 11:113–127.
15. Wang DO, Martin KC, Zukin RS (2010) Spatially restricting gene expression by local translation at synapses. *Trends Neurosci* 33:173–182.
16. Lake JA (1985) Evolving ribosome structure: Domains in archaebacteria, eubacteria, eocytes and eukaryotes. *Annu Rev Biochem* 54:507–530.
17. Gross B, Westermann P, Bielka H (1983) Spatial arrangement of proteins within the small subunit of rat liver ribosomes studied by cross-linking. *EMBO J* 2:255–260.
18. Marion MJ, Marion C (1987) Localization of ribosomal proteins on the surface of mammalian 60S ribosomal subunits by means of immobilized enzymes. Correlation with chemical cross-linking data. *Biochem Biophys Res Commun* 149:1077–1083.
19. Lutsch G, et al. (1990) Immunoelectron microscopic studies on the location of ribosomal proteins on the surface of the 40S ribosomal subunit from rat liver. *Eur J Cell Biol* 51:140–150.
20. Pisarev AV, et al. (2008) Ribosomal position and contacts of mRNA in eukaryotic translation initiation complexes. *EMBO J* 27:1609–1621.
21. Verschoor A, Srivastava S, Grassucci R, Frank J (1996) Native 3D structure of eukaryotic 80S ribosome: Morphological homology with the *E. coli* 70S ribosome. *J Cell Biol* 133:495–505.
22. Spahn CM, et al. (2001) Structure of the 80S ribosome from *Saccharomyces cerevisiae*-tRNA-ribosome and subunit–subunit interactions. *Cell* 107:373–386.
23. Chandramouli P, et al. (2008) Structure of the mammalian 80S ribosome at 8.7 A resolution. *Structure* 16:535–548.
24. Taylor DJ, et al. (2009) Comprehensive molecular structure of the eukaryotic ribosome. *Structure* 17:1591–1604.
25. Alkemar G, Nygård O (2006) Probing the secondary structure of expansion segment ES6 in 18S ribosomal RNA. *Biochemistry* 45:8067–8078.
26. Armache J-P, et al. (2010) Localization of eukaryote-specific ribosomal proteins: Implications for structure, function and evolution. *Proc Natl Acad Sci USA* 10.1073/pnas.1010005107.
27. Becker T, et al. (2009) Structure of monomeric yeast and mammalian Sec61 complexes interacting with the translating ribosome. *Science* 326:1369–1373.
28. Bhushan S, et al. (2010) α-Helical nascent polypeptide chains visualized within distinct regions of the ribosomal exit tunnel. *Nat Struct Mol Biol* 17:313–317.
29. Ban N, et al. (1999) Placement of protein and RNA structures into a 5 Å-resolution map of the 50S ribosomal subunit. *Nature* 400:841–847.
30. Clemons WMJ, et al. (1999) Structure of a bacterial 30S ribosomal subunit at 5.5 Å resolution. *Nature* 400:833–840.
31. Seidelt B, et al. (2009) Structural insight into nascent polypeptide chain-mediated translational stalling. *Science* 326:1412–1415.
32. Jossinet F, Ludwig TE, Westhof E (2010) Assemble: an interactive graphical tool to analyze and build RNA architectures at the 2D and 3D levels. *Bioinformatics* 26:2057–2059.
33. Stombaugh J, Zirbel CL, Westhof E, Leontis NB (2009) Frequency and isostericity of RNA base pairs. *Nucleic Acids Res* 37:2294–2312.
34. Hofacker IL (2003) Vienna RNA secondary structure server. *Nucleic Acids Res* 31:3429–3431.
35. Steffen P, et al. (2006) RNAshapes: An integrated RNA analysis package based on abstract shapes. *Bioinformatics* 22:500–503.
36. Trabuco LG, et al. (2008) Flexible fitting of atomic structures into electron microscopy maps using molecular dynamics. *Structure* 16:673–683.
37. Gerbi SA (1996) *Ribosomal RNA—Structure, Evolution, Processing, and Function in Protein Synthesis*, eds RA Zimmermann and AE Dahlberg (CRC, Boca Raton, FL), pp 71–87.
38. Lecompte O, et al. (2002) Comparative analysis of ribosomal proteins in complete genomes: An example of reductive evolution at the domain scale. *Nucleic Acids Res* 30:5382–5390.
39. Beckmann R, et al. (2001) Architecture of the protein-conducting channel associated with the translating 80S ribosome. *Cell* 107:361–372.
40. Sweeney R, Chen LH, Yao MC (1994) An rRNA variable region has an evolutionarily conserved essential role despite sequence divergence. *Mol Cell Biol* 14:4203–4215.
41. Cannone JJ, et al. (2002) The comparative RNA web (CRW) site: An online database of comparative sequence and structure information for ribosomal, intron, and other RNAs. *BMC Bioinformatics* 3:1–31.
42. Dube P, et al. (1998) The 80S rat liver ribosome at 25 A resolution by electron cryomicroscopy and angular reconstitution. *Structure* 6:389–399.
43. Morgan DG, et al. (2000) A comparison of the yeast and rabbit 80S ribosome reveals the topology of the nascent chain exit tunnel, inter-subunit bridges and mammalian rRNA expansion segments. *J Mol Biol* 301:301–321.
44. Spahn CM, et al. (2004) Cryo-EM visualization of a viral internal ribosome entry site bound to human ribosomes; the IRES functions as an RNA-based translation factor. *Cell* 118:465–475.
45. Erickson AH, Blobel G (1983) Cell-free translation of messenger RNA in a wheat germ system. *Method Enzymol* 96:38–50.
46. Halic M, et al. (2004) Structure of the signal recognition particle interacting with the elongation-arrested ribosome. *Nature* 427:808–814.
47. Wagenknecht T, et al. (1988) Direct localization of the tRNA-anticodon interaction site on the *Escherichia coli* 30S ribosomal subunit by electron microscopy and computerized image averaging. *J Mol Biol* 203:753–760.
48. Mindell JA, Grigorieff N (2003) Accurate determination of local defocus and specimen tilt in electron microscopy. *J Struct Biol* 142:334–347.
49. Frank J, et al. (1996) SPIDER and WEB: Processing and visualization of images in 3D electron microscopy and related fields. *J Struct Biol* 116:190–199.
50. Penczek PA, Frank J, Spahn CM (2006) A method of focused classification, based on the bootstrap 3D variance analysis, and its application to EF-G-dependent translocation. *J Struct Biol* 154:184–194.
51. Schuwirth B, et al. (2005) Structures of the bacterial ribosome at 3.5 Å resolution. *Science* 310:827–834.
52. Villa E, et al. (2009) Ribosome-induced changes in elongation factor Tu conformation control GTP hydrolysis. *Proc Natl Acad Sci USA* 106:1063–1068.
53. Jossinet F, Westhof E (2005) Sequence to structure (S2S): Display, manipulate and interconnect RNA data from sequence to structure. *Bioinformatics* 21:3320–3321.
54. Leontis NB, Westhof E (2001) Geometric nomenclature and classification of RNA base pairs. *RNA* 7:499–512.
55. Tamura M, et al. (2004) SCOR: Structural classification of RNA, version 2.0. *Nucleic Acids Res* 32:182D–184.
56. Pettersen EF, et al. (2004) UCSF Chimera—a visualization system for exploratory research and analysis. *J Comput Chem* 25:1605–1612.
57. Humphrey W, Dalke A, Schulten K (1996) VMD—visual molecular dynamics. *J Mol Graphics* 14:33–38.
58. Grayson P, Tajkhorshid E, Schulten K (2003) Mechanisms of selectivity in channels and enzymes studied with interactive molecular dynamics. *Biophys J* 85:36–48.
59. Alkemar G, Nygård O (2003) A possible tertiary rRNA interaction between expansion segments ES3 and ES6 in eukaryotic 40S ribosomal subunits. *RNA* 9:20–24.